Int. J. Solids Structures Vol. 29, No. 21, pp. 2649–2668, 1992
Printed in Great Britain.

0020–7683/92 $5.00+.00

ANALYSIS OF FIBER MOTION DURING WET FILAMENT WINDING OF COMPOSITE CYLINDERS WITH ARBITRARY THICKNESS

A. AGAH-TEHRANI† and H. TENG
Department of Theoretical and Applied Mechanics, University of Illinois at Urbana-Champaign, Urbana, IL 61801, U.S.A.

(*Received* 1 *February* 1991; *in revised form* 28 *December* 1991)

Abstract—A continuum consolidation model is proposed for macroscopic analysis of fiber motion during filament winding of thermoset composite cylinders with arbitrary thickness. The model takes account of the variation of both instantaneous stiffness and permeability of the mixture with fiber compaction. Due to resin filtration, structure of the resulting initial-boundary value problem is similar to that of a moving boundary problem. Based on this analogy, a finite difference scheme is devised for the solution of the problem. For the case of winding onto a rigid mandrel, the results point to the existence of an active and a passive zone of consolidation. The results further indicate the possibility that during hoop winding of relatively thick cylinders, the tension can be completely lost in the portion of the passive zone away from the mandrel.

1. INTRODUCTION

The filament winding is a manufacturing process which can be used for forming composite cylinders with high strength. The essence of this processing method is to successively add layers with different winding angles onto a moderately stiff cylinder which is invariably circular (mandrel). The layers may be wrapped in adjacent bands or in repeating patterns which eventually cover the surface of the mandrel. The winding angle may vary from longitudinal (parallel to the axis of the mandrel) to circumferential (perpendicular to the axis of the mandrel). The binder is a thermoset resin which can be epoxy, polyester or vinyl ester. If the thermoset resin is mixed with the fiber bundle during the winding stage, one has wet winding. Alternatively, if pre-impregnated B-staged form of the mixture of resin and fiber bundle is used, one has dry winding [for an exhaustive discussion of filament winding see Shilbey (1982)]. For a given composite system, the primary control variables during winding can be identified as: the tension applied to each layer, the velocity of the machine which traverses along the axis of the mandrel (cross-head velocity), and the angular velocitiy of the mandrel (Calius and Springer, 1985). The end result of the forced winding stage will be the development of a system of compressive radial and tensile circumferential stresses within the cylinder. In the case of wet winding, one also has the consolidation of the fiber network.

Following the winding stage, the wound cylinder is initially cured at elevated temperatures so as to cause cross-linking of the resin, and then it is cooled down to ambient temperature. During the heat build-up, such phenomena as micro- and macroflow of the binder, thermal expansion and simultaneous decrease in stiffness in the transverse direction, partial relaxation of the winding stresses, and change in the winding pressure on the mandrel due to mismatch in thermal expansion coefficients of the mandrel and the cylinder take place. The difference in the thermal expansion coefficient of a semifabricated material and the mandrel leads to an increase in the winding pressure on the mandrel. The decrease in stiffness and intensification of dissipation phenomena lead to the opposite effect with the second mechanism usually prevailing. Upon polymerization, the increase in strength and stiffness in the transverse direction together with the chemical shrinkage take place preferentially in the same direction, while slight relaxation of the winding stresses continues. The balance between these two competing mechanisms leads to the winding pressure on

†Currently, Lecturer at the Department of Mechancial Engineering, San Diego State University, San Diego, CA 92182-0191, U.S.A.

the mandrel remaining constant during polymerization. Alternatively one can envisage the case where curing is accomplished during winding. In such a case, the rate of heating the mandrel should also be considered as one of the control variables.

Upon cooling, while the processes of creep and stress relaxation continue, thermal shrinkage and increase in stiffness in the transverse direction take place. The winding pressure on the mandrel changes due to the difference in coefficients of thermal expansion between the mandrel and the cured article. This is in contrast to that during the heat build-up. In the present case, the nature of the competition between the two mechanisms is different. The free strain caused by the change in stiffness of the cured material upon cooling under conditions of finite stress is smaller than the thermal shrinkage strain. Therefore, the contribution of thermal shrinkage is dominant and upon cooling the radial compressive stresses decrease and in some cases regions of tensile radial stress develop.

In order to predict the occurrence of damage in the final product which is often in the form of the fiber waviness (due to the circumferential buckling) or the transverse cracks (due to the tensile radial stress) in between the layers, there is a need for a reliable method for predicting the state of the composite cylinder at the end of each of the three stages of the manufacturing process: (1) winding, (2) curing and (3) final cool-down. An important attribute of each submodel must be its ability to predict the stresses which are generated during the corresponding stage. In the case of wet winding, one must also be able to determine the radial distribution of the fiber volume fraction which arises as the result of the settling of fiber bundles in the liquid resin.

By assuming that successive layers are wrapped simultaneously on the mandrel, one can utilize the existing models for stess analysis of tape winding (Willett and Poesch, 1988; Lin and Westmann, 1989) in order to simulate the dry winding. In so doing, one is neglecting the fact that in reality the layers are wrapped sequentially next to each other resulting in the axial variation of the outer radius. The analogy can be further completed by observing that dry winding is a generalized plane strain problem while tape winding is a plane stress problem.

Irrespective of the thickness of the wound cylinder, theoretical modelling of wet winding must take account of the resin filtration through the fiber bundles which is induced by the existing pressure gradient. Recently Calius and Springer (1990) have outlined a model for simulating the entire stages of wet winding. Their submodel related to the forced winding stage, which neglects radial resistance of the fiber network, is based on considering the force equilibrium and the conservation of mass within each layer. Although this model is only appropriate for thin cylinders where one can neglect the increase in the radial stiffness and the decrease in permeability of the fiber bundles due to consolidation, it does allow for arbitrary orientation of the fiber bundle. Lee and Springer (1990) by basing their stress submodel on a continuum formulation have extended the model by Calius and Springer for analysing filament winding of thick cylinders. An important characteristic of the Lee–Springer model is the assumption that consolidation takes place only in the last layer. This *a priori* assumption for the fiber motion is only valid if the time scale associated with the winding of each layer is exceedingly large compared to the time constant of the resin filtration through the fiber bundle. It must be mentioned that different filament winding models proposed by Springer and co-workers are the only models which provide a unified view of this complicated manufacturing process.

Within the framework of a discretized consolidation model, one must mention the work by Bolotin *et al.* (1980) who have included the elasticity of the fiber network by introducing the term associated with the radial pliability in the equilibrium of the layers whose thickness is below the critical value at which the radial resistance arises.

Any comprehensive model for analysing fiber motion during wet filament winding must take account of two important aspects which are associated with fiber compaction: (1) increase in the radial stiffness of the composite (Gutowski *et al.*, 1987a,b), and (2) reduction in the permeability (Gutowski *et al.*, 1987a,b; Gebart, 1990). The significance of these attributes becomes particularly apparent when the thickness of the cylinder becomes large. The primary aim of this paper is to provide a *continuum consolidation model* for analysing the wet winding of thermoset composite cylinders with arbitrary thickness which

incorporates the above characteristics. Such a model is developed by utilizing the rate form of Biot's consolidation mixture theory (Biot, 1941). In comparison with the existing discretized consolidation model purposed by Bolotin *et al.* (1980), the present formulation has two distinct advantages: One is that it is based on a continuous model, and the other is that it takes account of the reduction of permeability with fiber compaction. Following the description of the key features of the model, the details of the numerical calculation and interpretation of the results will be presented. The article will be concluded by a discussion on the importance of including the dependence of the radial resistance and permeability on fiber volume fraction in the analysis of wet winding.

2. DEVELOPMENT OF THE MODEL

The composite cylinder is assumed to be a mixture of incompressible fluid (resin) and solid (fiber bundle). The fiber bundles are assumed to be in the hoop direction. The axial flow of the resin due to the time delay in winding along the axis of the cylinder will be neglected, i.e. it is assumed that all layers along the axis of the cylinder are laid simultaneously. Moreover, the angular variation of the outer radius due to the helical nature of the winding will also be neglected, see Fig. 1. Because of these two assumptions, the only non-vanishing component of the velocity of each phase will be the radial velocity, and the problem becomes one-dimensional in space. In order to facilitate the analysis, the following non-dimensional group of parameters are introduced:

$$x = \frac{r}{R_i}, \quad \tilde{u}_s = R_i u_s, \quad \tilde{u}_f = R_i u_f, \quad \lambda = \frac{C^o_{rr}}{C^o_{\theta\theta}}, \quad \beta = \frac{C^o_{r\theta}}{C^o_{\theta\theta}},$$

$$y = \frac{\kappa^o C^o_{\theta\theta}}{R_i^2} t, \quad (\tilde{\sigma}_{rr}, \tilde{\sigma}_{\theta\theta}, \tilde{p}) = C^o_{\theta\theta}(\sigma_{rr}, \sigma_{\theta\theta}, p), \tag{1}$$

where R_i is the outer radius of the mandrel, r is the dimensional radial coordinate, $\tilde{u}_s$ and $\tilde{u}_f$ are radial displacements of the solid and fluid phase, C^o_{rr} and $C^o_{\theta r}$ are the moduli of the fiber network which has reached the maximum achievable fiber volume fraction and $C^o_{\theta\theta}$ is the hoop stiffness of an individual fiber, $\tilde{\sigma}_{rr}$ and $\tilde{\sigma}_{\theta\theta}$ are, respectively, the radial and the hoop stress components of the mixture, $\tilde{p}$ is the partial pressure of the resin, t denotes time and κ^o is the permeability as the fiber bundle passes through the resin bath.

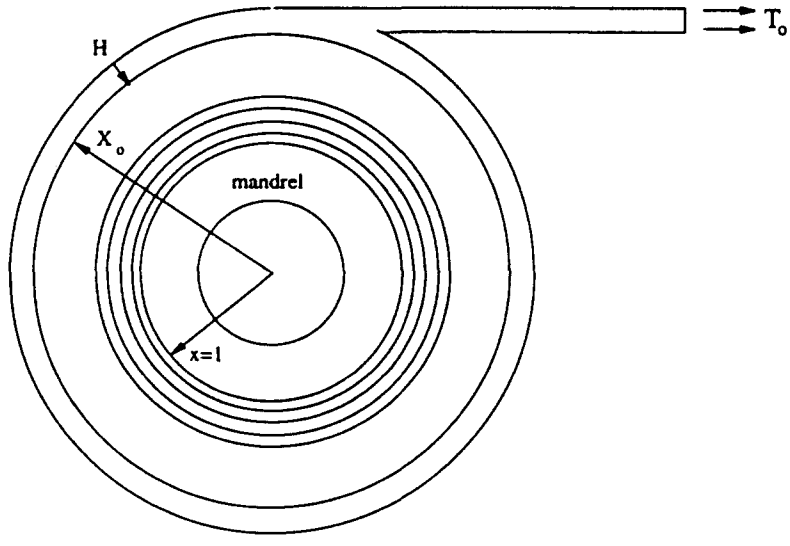

Fig. 1. Geometry of the model.

By utilizing the above non-dimensional relations, one can determine the following expressions for the non-dimensional velocities of the fiber network and the resin denoted respectively by w_s and w_f†

$$w_s = \frac{\partial u_s}{\partial y} = \frac{t_f}{R_i}\frac{\partial \tilde{u}_s}{\partial t}, \qquad w_f = \frac{\partial u_f}{\partial y} = \frac{t_f}{R_i}\frac{\partial \tilde{u}_f}{\partial t}, \tag{2, 3}$$

with $t_f = R_i^2/\kappa^o C_{\theta\theta}^o$ as the characteristic time for filtration. The definition of t_f indicates that increasing κ^o reduces the characteristic time for filtration and hence the time for consolidation.

The dependence of the instantaneous moduli of the fiber bundle $C_{\xi\eta}$ and the instantaneous permeability of the fiber network on fiber volume fraction ϕ_s are assumed to be of the form given below

$$(C_{rr}, C_{r\theta}) = F(\phi_s)(C_{rr}^o, C_{r\theta}^o), \quad C_{\theta\theta} = \phi_s C_{\theta\theta}^o, \quad \kappa = \kappa^o G(\phi_s). \tag{4, 5}$$

The values of the moduli C_{rr}^o and $C_{\theta\theta}^o$ and the functions $F(\phi_s)$ and $G(\phi_s)$ must be determined from experiments on fiber compaction (Gutowski *et al.*, 1987b; Gebart, 1990). It should be noted that for simplicity we have assumed identical dependence of C_{rr} and $C_{\theta\theta}$ on the fiber volume fraction ϕ_s.

In terms of the apparent density of the phases ($\rho_i = m_i/\forall_i, i = s, f$), the conservation of mass for the fluid and the solid phase can be written as (Bowen, 1976; Kenyon, 1976)

$$\frac{\partial \rho_f}{\partial y} + \nabla \cdot [\rho_f w_f] = 0, \qquad \frac{\partial \rho_s}{\partial y} + \nabla \cdot [\rho_s w_s] = 0, \tag{6, 7}$$

with ∇ denoting the gradient operator.

By assuming that the densities of both solid and fluid phases remain constant during deformation, (6) and (7) can be manipulated to obtain the following expressions for the conservation of mass in terms of the volume fractions of individual phases ($\phi_i = \rho_i \forall_i / m_i$, $i = f, s$)

$$\frac{\partial \phi_f}{\partial y} + \nabla \cdot [\phi_f w_f] = 0, \qquad \frac{\partial \phi_s}{\partial y} + \nabla \cdot [\phi_s w_s] = 0. \tag{8, 9}$$

Addition of the above two relations, and usage of the identity $\phi_f + \phi_s = 1$ leads to the final desired form of the conservation of mass which involves only the velocitiy of the solid and the filtration flux $q = \phi_f(w_f - w_s)$ (the surface integral of q over the outer radius of the cylinder is the amount of the fluid leaving the mixture). By enforcing the condition that no resin passes through the mandrel ($q(1, y) = 0$), the resultant expression can be integrated to obtain

$$q = -w_s + \frac{1}{x} g(y), \tag{10}$$

where $g(y)$ is the velocity of the interface between the mandrel and the composite. We assume that the mandrel undergoes a small deformation so that changes in the outer radius of the mandrel can be neglected.

Conservation of mass analysis enables one to determine the evolution equation which governs the change in the fiber volume fraction. To obtain such a relation, one can simply rearrange the terms in (9) to get

$$\frac{d\phi_s}{dy} = -\phi_s[\nabla \cdot w_s], \tag{11}$$

† It is important to note that these are the velocities of a continuum point which contains the two phases.

where d/d_y represents the total derivative. The above equation by itself does not contain the property that the fiber volume fraction should not exceed the achievable volume fraction. In other words, if $w_s < 0$, the above expression does not provide any upper bound on the value of ϕ_s. However, it is understood that although the achievable fiber volume fraction ϕ_a varies with the packing geometry, it can never exceed one. This constraint implies that as $\phi_s \to \phi_a$, $w_s \to 0$. As will be indicated later, this constraint will be satisfied if the variation of permeability with fiber volume fraction is taken into account.

Since during wet winding the radial resistance of the layer just being wound on the mandrel is very small, the resin material can flow through the fiber network leading to increases in both the fiber volume fraction and the radial stiffness of the composite. Because of the finite changes in the fiber volume fraction, one needs to distinguish between the initial and the instantaneous configuration of the mixture. In so doing, we can either follow the motion of the fluid particle (resin) or the solid particle (fiber network). Since the final radius of the composite cylinder depends on the position of the last fiber layer which is being wound on the mandrel, the instantaneous configurations of the mixture and the solid phase are considered to be identical. Thus, $\sigma_{rr}(x, y)$ and $\sigma_{\theta\theta}(x, y)$ are the stress components of a mixture point at "time" y which is occupying the position x of the solid phase. In conjunction with this, we adopt an "updated-Langrangian" formulation to describe the motion of the mixture, that is at each instant of time the current configuration of the solid phase is considered to be the initial configuration of the mixture.

Due to the variation of the outer radius with time, the constitutive behavior of the solid phase and Darcy's Law are, respectively, expressed in the following rate form:

$$\dot{\sigma}_{rr} + \dot{p} = F(\phi_s)\left[\lambda \frac{\partial w_s}{\partial x} + \beta \frac{w_s}{x}\right], \qquad \dot{\sigma}_{\theta\theta} + \dot{p} = F(\phi_s)\beta \frac{\partial w_s}{\partial x} + \phi_s \frac{w_s}{x}, \tag{12, 13}$$

$$q = -G(\phi_s)\frac{\partial p}{\partial x}, \tag{14}$$

where $\dot{(\ )} = \partial/\partial y$ and p is the resin pressure in the current configuration.

The presence of the term $G(\phi_s)$ in (14) implies that as $G(\phi_s) \to 0$, the filtration flux approaches zero (fiber compaction comes to a halt). For the case of the rigid mandrel $[g(y) = 0]$, it immediately follows that the velocity of the solid will also approach zero. Thus, we have shown that at least when the mandrel is rigid, considering the variation of the permeability with ϕ_s leads to a bound on the fiber volume fraction. Further limitation on the increase in compaction can be achieved by incorporating the variation of radial stiffness with fiber volume fraction. This can be easily explained by observing that the compaction will be suppressed once it has reached a level where the radial stiffness of the fiber network is no longer negligible.

Substitution of (10) through (14) into the rate equilibrium equation in the radial direction

$$\frac{\partial \dot{\sigma}_{rr}}{\partial x} + \frac{\dot{\sigma}_{rr} - \dot{\sigma}_{\theta\theta}}{x} = 0, \tag{15}$$

leads to the following parabolic partial differential equation (PDE) for w_s

$$\frac{\partial}{\partial y}\left[\frac{w_s}{G(\phi_s)}\right] = F(\phi_s)\lambda\left[\frac{\partial^2 w_s}{\partial x^2} + \frac{1}{x}\frac{\partial w_s}{\partial x}\right] - \phi_s \frac{w_s}{x^2} + \frac{dF(\phi_s)}{d\phi_s}\frac{\partial \phi_s}{\partial x}\left(\lambda \frac{\partial w_s}{\partial x} + \beta \frac{w_s}{x}\right) + \frac{1}{x}\frac{\partial}{\partial y}\left[\frac{g(y)}{G(\phi_s)}\right]. \tag{16}$$

The value of the function $F(\phi_s)$ will be very small (close to zero) near the outer layer (where fiber compaction has not taken place), while in the inner layers where enough

compaction has occurred it will have a finite value. Because of this, the above equation is an example of a singularly perturbed PDE.

3. BOUNDARY CONDITIONS

The formulation of the problem will be completed by providing the necessary and sufficient boundary conditions for solving (16). The first boundary condition derived will be that associated with the rate of change of the fluid pressure at the instantaneous outer radius x_o. This can be accomplished by first substituting (10) into (14), integrating the resultant equation, and enforcing the boundary condition that at $p(x = x_o, y) = 0$ for all time, y. The end result will be

$$p(x, y) = \int_{x_o}^{x} \frac{1}{G(\phi_s)} \left[w_s(\xi, y) - \frac{g(y)}{\xi} \right] d\xi. \tag{17}$$

Based on the above expression and (16), the material derivative of resin pressure will be

$$\dot{p}(x, y) = -\frac{dx_o}{dy} \left[\frac{w_s(x_o, y)}{G(\phi_s^o)} - \frac{1}{x_o} \frac{g(y)}{G(\phi_s^o)} \right] + \int_{x_o}^{x} \left[F(\phi_s) \frac{\lambda - \beta}{\xi} \frac{\partial w_s}{\partial \xi} - \frac{\phi_s - F(\phi_s)\beta}{\xi^2} w_s \right] d\xi + F(\phi_s) \left(\lambda \frac{\partial w_s}{\partial x} + \beta \frac{w_s}{x} \right) \Bigg|_{x_o}^{x}, \tag{18}$$

where ϕ_s^o is the fiber volume fraction in the layer just being wound.

Following Lin and Westmann (1989), we let the amount the material added to the cylinder during the winding of each layer be

$$d(\text{Vol/unit length}) = 2\pi x_o \, dx = \bar{w}_o(y) \, dy H, \tag{19}$$

with H as the thickness of each fiber network just being wound, and $\bar{w}_o$ as the speed of the last layer. In considering different possibilities for the variation of $\bar{w}_o$ with "time" y, one can recognize two special cases: one in which $\bar{w}_o(y) =$ constant, and the other in which the angular velocity is held constant.

If the amount of resin filtration is small, then changes in the geometry can be neglected and (19) can be integrated to determine the outer radius as a function of time. Indeed, this is the approach adopted during the elastic or viscoelastic analysis of winding (Willett and Poesch, 1988; Lin and Westmann, 1989). In the current problem where resin filtration leads to changes in the position of the fiber network, eqn (19) will be interpreted with respect to instantaneous current configuration of the fiber network. In this case (19) leads to

$$\frac{dx_o}{dy} = \frac{\bar{w}_o H}{2\pi x_o}. \tag{20}$$

The above relation brings out the second important time scale in the problem which is associated with the speed at which the outer layer is increased. We define this time scale to be $t_w = R_i / w_o$ with w_o as the dimensional speed of the last layer.

The fact that at each increment of time the evolution of the outer radius of the composite (the position of outermost fiber network) is not known *a priori* indicates that the wet winding problem is in some sense an example of a moving boundary problem, and one needs to sequentially integrate the velocity equilibrium equation (16) for each instant of time in order to obtain the relevant information at the end of the winding process. To accomplish this one needs two boundary conditions on either the velocity or the strain rate of the solid, or a mixed combination of both [recall that (16) was 2nd order in the radial direction]. These boundary conditions can be obtained by considering the continuity of

traction and velocity across the mandrel/composite interface

$$\dot{\sigma}_{rr}(x=1, y) = \frac{E_m}{C_{\theta\theta}} \frac{R_i^2 - R_m^2}{R_i^2(1-\nu_m) + R_m^2(1+\nu_m)} g(y), \tag{21}$$

with R_m as the inner radius of the mandrel and (E_m, ν_m) as the elastic constants of the mandrel and utilizing the equilibrium of the last layer keeping the hoop stress constant and equal to the applied tension

$$\dot{\sigma}_{rr}(x = x_o, y) = -\frac{T_o}{x_o}\frac{dx_o}{dy}, \tag{22}$$

with T_o as the non-dimensional applied tension. (The non-dimensionalization is with respect to $C^o_{\theta\theta}$).

By utilizing (12) and (18), the boundary condition at $x = x_o$ becomes

$$-\frac{T_o}{x_o}\frac{dx_o}{dy} = \frac{dx_o}{dy}\left[\frac{w_s(x_o, y)}{G(\phi_s^o)} - \frac{1}{x_o}\frac{g(y)}{G(\phi_s^o)}\right] + F(\phi_s)\left(\lambda\frac{\partial w_s}{\partial x} + \beta\frac{w_s}{x}\right)\Bigg|_{x=x_o}, \tag{23}$$

while the boundary condition at $x = 1$ becomes

$$-\frac{T_o}{x_o}\frac{dx_o}{dy} = E'_m g(y) - \int_1^{x_o}\left[F(\phi_s)\frac{\lambda-\beta}{\xi}\frac{\partial w_s}{\partial \xi} - \frac{\phi_s - F(\phi_s)\beta}{\xi^2} w_s\right] d\xi, \tag{24}$$

with

$$E'_m = \frac{E_m}{C_{\theta\theta}} \frac{R_i^2 - R_m^2}{R_i^2(1-\nu_m) + R_m^2(1+\nu_m)}.$$

The fact that the variation of the outer radius with time is unknown provides an additional difficulty in wet winding analysis which is absent in the analysis of either linear-elastic or viscoelastic dry winding. This difficulty is related to the fact that in wet winding satisfaction of the boundary conditions leads to an eigenvalue problem involving the outer radius. This dependence implies that, unlike the linear dry winding problems, superposition of solutions in wet winding corresponding to different outer radii leads to an error in satisfying force equilibrium.

4. NUMERICAL FORMULATION

One major source of biased errors during integration of (16) in time is the lack of equilibrium at the end of each increment. In order to eliminate this type of error, (15) is modified in the following manner.

$$\frac{\partial \dot{\sigma}_{rr}(x, y+\Delta y)}{\partial x} + \frac{\dot{\sigma}_{rr}(x, y+\Delta y) - \dot{\sigma}_{\theta\theta}(x, y+\Delta y)}{x} + \frac{1}{\Delta y}\left[\frac{\partial \sigma_{rr}(x, y)}{\partial x} + \frac{\sigma_{rr}(x, y) - \sigma_{\theta\theta}(x, y)}{x}\right] = 0, \tag{25}$$

with the stress rates at time $y+\Delta y$ being related to radial velocity at that time through the constitutive relations (12) and (13). The term inside the bracket represents the residual body force at time $y+\Delta y$ due to the lack of equilibrium at time y. The above equation can also be interpreted as the force equilibrium at time $y+\Delta y$ in terms of the stress rates at that time and the total stresses at the previous time.

The form of the modified rate equilibrium equation (25) readily renders itself to Euler backward method (an implicit algorithm) for integration in time. A finite difference scheme was then used to replace the spatial derivatives. Since the solution of the problem requires the ability to follow the history of winding from beginning ($y = 0$) to end ($y = y_f$), the size of the finite difference mesh was sequentially increased as time increased, see Fig. 2. Due to the change in the geometry which is induced by the resin filtration, the sequential increase in mesh size resulted in non-uniform mesh spacing. By applying Richardson extrapolation (Dahlquist and Bjorck, 1974) to the midpoint rule, the first and second order spatial derivatives of the interior nodes can be obtained as

$$\left|\frac{\partial}{\partial x}\right|_{x_m} = d_m(\ )_{m+1} + f_m(\ )_{m-1} + e_m(\ )_m, \tag{26}$$

$$\left|\frac{\partial^2}{\partial x^2}\right|_{x_m} = \frac{2}{l_m}[h_{m-1}(\ )_{m+1} + h_m(\ )_{m-1} - (h_m + h_{m-1})(\ )_m], \tag{27}$$

where

$$d_m = \frac{h_{m-1}^2}{l_m}, \quad f_m = -\frac{h_m^2}{l_m}, \quad e_m = \frac{h_m^2 - h_{m-1}^2}{l_m}, \quad h_m = x_{m+1} - x_m,$$
$$l_m = h_m h_{m-1}[h_m + h_{m-1}]. \tag{28}$$

Similar expressions can also be derived for the boundary nodes. Due to the large variations that the function $F(\phi_s)$ can experience, the governing equation for w_s will be stiff. In order to reduce the limitation that this stiffness imposes on the time increment for stable integration, we proceed in the following manner. First, we integrate the evolution equation for the fiber volume fraction (11) between the time $y > y_n$ and $y = y_n$. The result will be

$$\ln\left(\frac{\phi_s(x, y)}{\phi_s(x, y_n)}\right) = -\int_{y_n}^{y}\left[\frac{\partial w_s}{\partial x} + \frac{w_s}{x}\right]dy. \tag{29}$$

By utilizing the above relation, one can then determine the following relation for the spatial derivative of fiber volume fraction

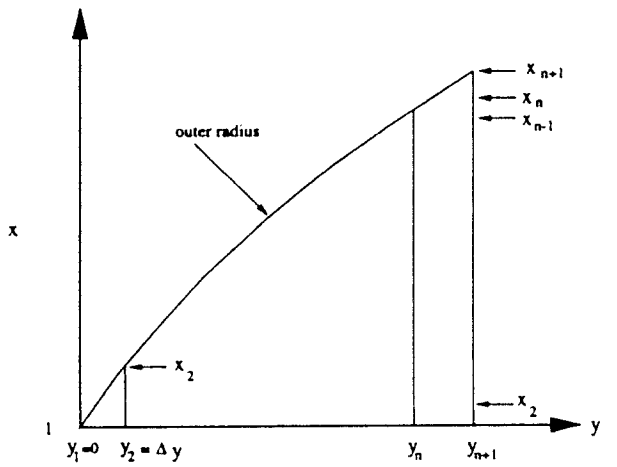

Fig. 2. Schematic of the finite difference mesh.

$$\frac{\partial \phi_s(x, y)}{\partial x} = \frac{\phi_s(x, y)}{\phi_s(x, y_n)} \frac{\partial \phi_s(x, y_n)}{\partial x} - \phi_s(x, y) \int_{y_n}^{y} \left(\frac{\partial^2 w_s}{\partial x^2} + \frac{1}{x} \frac{\partial w_s}{\partial x} - \frac{w_s}{x^2} \right) dy. \tag{30}$$

The final step in obtaining the finite difference equation of the original PDE will be to substitute (30) into (16), and then into (25). By utilizing the midpoint rule, integration of the resultant equation between the time $y = y_n$ and $y = y_{n+1}$ leads to

$$\frac{1}{\Delta y}\left[\frac{W_m^{n+1}}{G_m^{n+1}} - \frac{W_m^n}{G_m^n}\right] = F_m^{n+1/2}\lambda[a_m W_{m+1}^{n+1} + b_m W_m^{n+1} + c_m W_{m-1}^{n+1}] - \phi_m^{n+1/2}\frac{W_m^{n+1}}{x_m^2}$$

$$+ F_m'^{n+1/2}\frac{\phi_m^{n+1/2}}{\phi_m^n}(d_m\phi_{m+1}^n + e_m\phi_m^n + f_m\phi_{m-1}^n)\left[\lambda d_m W_{m+1}^{n+1} + \left(\lambda e_m + \frac{\beta}{x_m}\right)W_m^{n+1} + \lambda f_m W_{m-1}^{n+1}\right]$$

$$- \tfrac{1}{4}F_m'^{n+1}\phi_m^{n+1}\Delta y\left[\lambda d_m \bar{W}_{m+1}^{n+1} + \left(\lambda e_m + \frac{\beta}{x_m}\right)\bar{W}_m^{n+1} + \lambda f_m \bar{W}_{m-1}^{n+1}\right]\left(a_m W_{m+1}^{n+1} + \left(b_m - \frac{1}{x_m^2}\right)\right.$$

$$\left.\times W_m^{n+1} + c_m W_{m-1}^{n+1}\right) - \tfrac{1}{4}F_m'^{n+1}\phi_m^{n+1}\Delta y\left(a_m W_{m+1}^n + \left(b_m - \frac{1}{x_m^2}\right)W_m^n + c_m W_{m-1}^n\right)$$

$$\times\left[\lambda d_m W_{m+1}^{n+1} + \left(\lambda e_m + \frac{\beta}{x_m}\right)W_m^{n+1} + \lambda f_m W_{m-1}^{n+1}\right] + \frac{1}{x_m \Delta y}\left[\frac{g^{n+1}}{G_m^{n+1}} - \frac{g^n}{G_m^n}\right] + \frac{1}{\Delta y}$$

$$\times\left[d_m\sigma_{rr(m+1)}^n + \left(e_m + \frac{1}{x_m}\right)\sigma_{rr(m)}^n + f_m\sigma_{rr(m-1)}^n - \frac{1}{x_m}\sigma_{\theta\theta(m)}^n\right], \quad \text{for} \quad 2 \leqslant m \leqslant n, \; 3 \leqslant n \tag{31}$$

where

$$a_m = \frac{2h_{m-1}}{l_m} + d_m, \quad c_m = \frac{2h_m}{l_m} + f_m, \quad b_m = \frac{-2(h_m + h_{m-1})}{l_m} + e_m,$$

and the superscripts specify the time and the subscripts specify the node numbers.

The boundary condition (23) is replaced by the following difference equation

$$-\frac{T_0}{x_{n+1}}\frac{dx_0}{dy} = \frac{dx_0}{dy}\frac{1}{G_{n+1}^{n+1}}\left[W_{n+1}^{n+1} - \frac{1}{x_{n+1}}g^{n+1}\right]$$

$$+ F_{n+1}^{n+1}\left[\lambda\bar{e}W_{n+1}^{n+1} + \left(\lambda\bar{d} + \frac{\beta}{x_{n+1}}\right)W_n^{n+1} + \lambda\bar{f}W_{n-1}^{n+1}\right], \tag{32}$$

with

$$\bar{d} = \frac{2h_n + h_{n-1}}{h_n(h_n + h_{n-1})}, \quad \bar{e} = -\frac{h_n + h_{n-1}}{h_n h_{n-1}}, \quad \bar{f} = \frac{h_n}{h_{n-1}(h_n + h_{n-1})}.$$

The finite difference equation of the original PDE (31), and that of the boundary condition (32) can be used to obtain the following systems of equations for the nodal velocities at time $y_{n+1} = y_n + \Delta y$

$$\mathbf{A}\mathbf{W}^{n+1} = \mathbf{B} + \mathbf{R}g^{n+1}, \tag{33}$$

where $\mathbf{W}^{n+1^T} = [W_2 \ldots W_n]^{n+1}$.

The coefficients of the tridiagonal matrix **A**, and the column matrices **B** and **R** are given in the Appendix. Based on the above finite difference formulation of the problem, the

strategy for the computation is as follows:

(1) For the first time increment, by assuming linear spatial variation of the velocity of solid w_s, the boundary conditions (23) and (24) are used to determine the nodal values of w_s.

(2) During the subsequent increments, the nodal velocities are obtained through a predictor-corrector method with each pass consisting of:

(i) Using (33) to obtain

$$\mathbf{W}^{n+1} = \mathbf{A}^{-1}[\mathbf{B} + \mathbf{R}g^{n+1}]. \tag{34}$$

(ii) Utilizing the boundary condition (24) to obtain the interface velocity g_{n+1}.

(iii) Determining the nodal velocities from (34), and hence the increments of stress, pressure and fiber volume fraction.

We used the total equilibrium equation in the radial direction to obtain the following estimate of the error associated with the numerical calculation

$$\text{error} = \frac{1}{\sigma_{\theta\theta}}\left[\frac{\mathrm{d}}{\mathrm{d}r}(r\sigma_{rr}) - \sigma_{\theta\theta}\right]. \tag{35}$$

5. DISCUSSION AND RESULTS

In this section by assuming specific forms for the functions $F(\phi_s)$ and $G(\phi_s)$, we will analyse the response of the proposed model. These forms are given as follows

$$F(\phi_s) = F^0(\phi_s - \phi_s^0)^5 + E^0, \qquad G(\phi_s) = G^0\left(\sqrt{\frac{\phi_a}{\phi_s}} - 1\right)^2, \tag{36, 37}$$

with ϕ_s^0 as the initial fiber volume fraction of the layer which is being wound onto the mandrel, $E^0 C_{rr}^0$ as the initial stiffness of that layer, and $G^0\kappa^0$ as its permeability. The constant F^0 is such that $F(\phi_a)C_{rr}^0$ will be the radial stiffness of the fiber network with the maximum possible volume fraction.

The form for $G(\phi_s)$, see Fig. 3, is chosen based on the expression derived by Gebart (1990) who showed that the variation of the transverse permeability of the mixture with

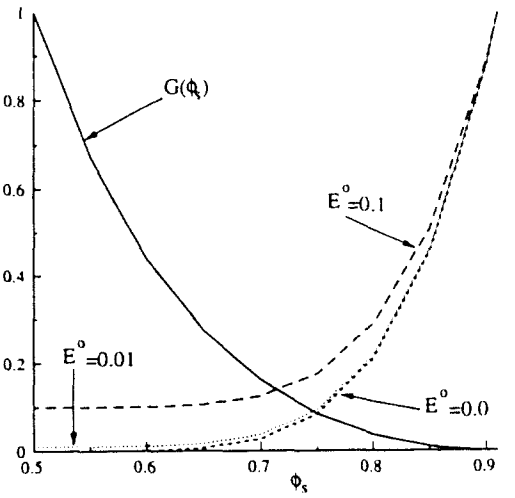

Fig. 3. Variation of the functions $G(\phi_s)$ and $F(\phi_s)$ with fiber volume fraction.

Table 1. The constants used in the numerical solution

Velocity of deposition w_0	0.256 m s^{-1}
Thickness of the last layer H	0.25 mm
Applied tension	10 MPa
Outside radius of the mandrel R_1	0.5 m
Hoop stiffness of the fiber $C^0_{\theta\theta}$	222 GPa
$C^0_{rr}/C^0_{\theta\theta}$	0.204
κ^0	2×10^{-13} m^2 Pa^{-1} s^{-1}
Initial fiber volume fraction ϕ_s^0	0.5

fiber volume fraction is fundamentally different from the variation of the axial permeability. The form of the function $F(\phi_s)$ is chosen so that the radial resistance will initially remain almost constant, see Fig. 3, and eventually equals C^0_{rr}. The above forms have the interesting feature that the drop in the permeability is faster than the rise in the radial stiffness. This implies that based on the assumed forms for the functions $F(\phi_s)$ and $G(\phi_s)$ even though compaction can be significantly reduced due to the decrease in the permeability, the radial stiffness can still be small.

The material constants and the value of the parameters associated with the winding process are given in Table 1. *In order to reduce the amount of computation involved, we have only considered winding onto a rigid mandrel.*

Initially, the variation of the radial stiffness with fiber volume fraction was neglected, see Figs 4–8, however the permeability of the mixture was allowed to vary with ϕ_s. This was done so as to investigate the influence of the radial stiffness on fiber compaction. The time increment for each calculation was $\Delta t = 0.2$ s. Time increments greater than this lead to significant error accumulation and eventual instabilitiy of the result. The results in Table 2 present the maximum errors in equilibrium which happen to occur in the outer mode.

The results in Fig. 4 show the variation of the fiber volume fraction through the thickness. As expected, this figure indicates that increasing the radial stiffness of the fiber network suppresses fiber compaction. The interesting feature of this figure is that for cases where the initial resistance of the fiber network is sufficiently small so as to allow significant compaction, there are two boundary-layers: one close to the mandrel–composite interface and the other close to the outer layer. In between these two layers fiber volume fraction is nearly constant†. Figure 5 presents the details inside the boundary layer close to $x = 1$. As the results indicate, the boundary layer becomes more diffused as the radial stiffness increases. In interpreting this figure, it is important to note that the length of the boundary layer is of the order of the thickness of an individual composite layer. Thus keeping in mind that fiber diameter is of the order of 10 μm, adopting the continuum approach in the manner presented in this study should be viewed with caution. Apart from the inner boundary layer which is dependent on the stiffness of the mandrel, the results presented in Figs 4 and 5 imply that the profile of the fiber volume fraction can be separated into a passive and an active zone of consolidation. Inside the passive zone the compaction due to the winding

Table 2. The maximum error for the cases where the radial stiffness was considered constant

Radial stiffness C^0_{rr}	Error
147.5 Pa	10.56 %
1.475 kPa	1.78 %
14.75 kPa	0.217 %
1.475 MPa	5.02×10^{-4}
0.1475 GPa	-4.52×10^{-5}

†Numerical results indicate a slight linear variation of the fiber volume fraction with radial position. The slope of this inner layer increases as the radial resistance of the fiber increases.

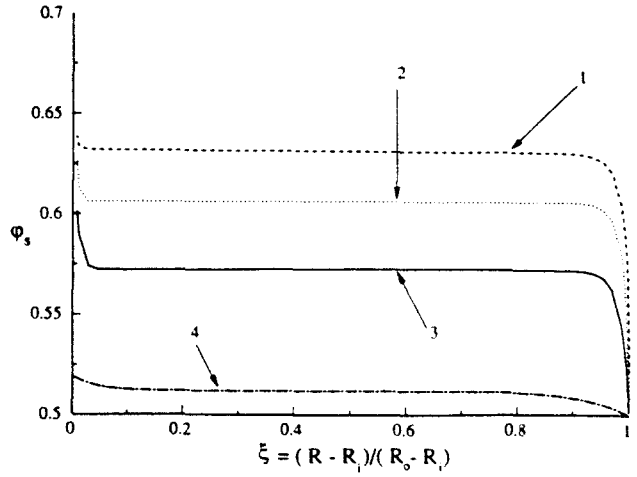

Fig. 4. Radial distribution of fiber volume fraction for the following cases: (1) C''_{rr} = 147.5 Pa. (2) C''_{rr} = 1.475 kPa. (3) C''_{rr} = 14.75 kPa. (4) C''_{rr} = 1.475 MPa.

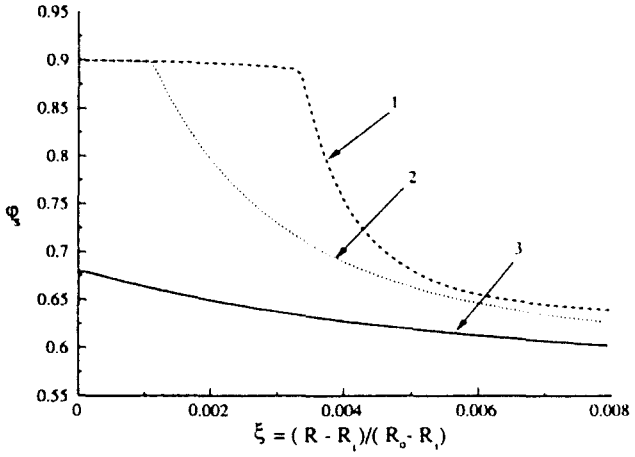

Fig. 5. Profile of fiber volume fraction in the boundary layer at the rigid interface between the mandrel and the composite for the following cases: (1) C''_{rr} = 147.5 Pa. (2) C''_{rr} = 1.475 kPa. (3) C''_{rr} = 14.75 kPa. C_{rr} = constant.

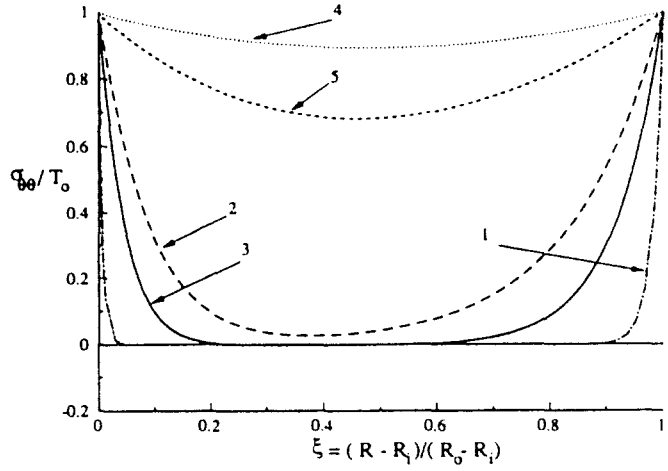

Fig. 6. Radial variation of the non-dimensional hoop stress for the following cases: (1) C''_{rr} = 14.75 kPa and n = 100 layers. (2) C''_{rr} = 1.475 MPa and n = 50 layers. (3) C''_{rr} = 1.475 MPa and n = 100 layers. (4) C''_{rr} = 0.1475 GPa and n = 50 layers. (5) C''_{rr} = 0.1475 GPa and n = 100 layers.

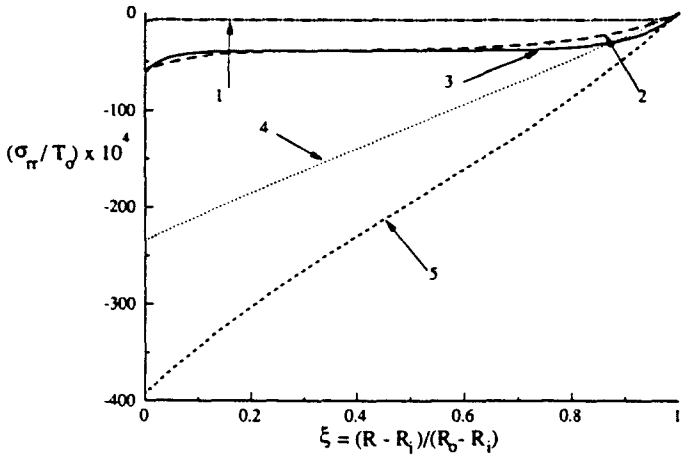

Fig. 7. Radial variation of the non-dimensional σ_{rr} for the following cases: (1) C^o_{rr} = 14.75 kPa and n = 100 layers. (2) C^o_{rr} = 1.475 MPa and n = 50 layers. (3) C^o_{rr} = 1.475 MPa and n = 100 layers. (4) C^o_{rr} = 0.1475 GPa and n = 50 layers. (5) C^o_{rr} = 0.1475 GPa and n = 100 layers.

tension has reached its saturation limit, while inside the active zone the compaction is still taking place. In cases (1) and (2) where the radial resistance of the fiber network was assumed to be small, the length of the active consolidating region came out to be seven to eight times the thickness of each ply.

Figure 6 shows the variation of the hoop stress in the composite cylinder. The results indicate that the drop in the hoop stress (loss in tension) increases by increasing the thickness of the cylinder. The loss in tension is more dramatic when the radial stiffness of the fiber is small. The drop in hoop stress can be explained by observing that each time a layer is added to the cylinder there will be a compressive hoop strain increment and a compressive radial strain increment. These compressive strain increments result in compressive hoop and radial stress increments. The larger the magnitude of anisotropy (the larger λ), the more compressive the hoop stress increment. Thus, as the degree of anisotropy increases, the loss of the initial winding tension increases. The results in Fig. 6 also indicate that in the case where the radial stiffness is very small (case 1), the hoop stress will be almost zero in the interior of the cylinder.

Figures 7 and 8, respectively, present the variation of the radial stress and the pressure through the thickness of the cylinder. The results in general indicate that increasing the

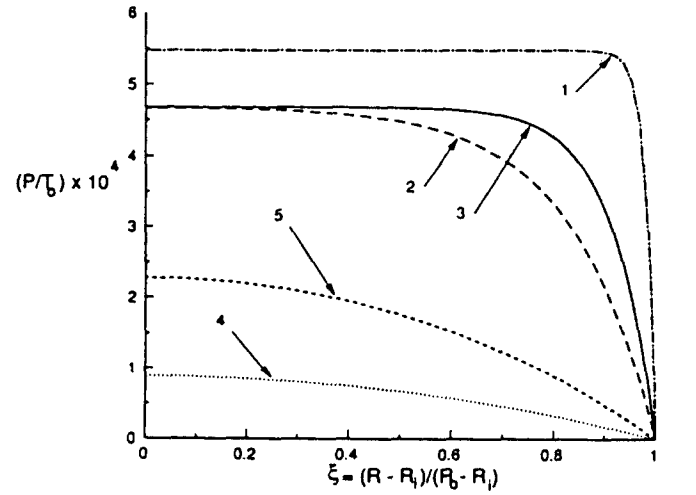

Fig. 8. Radial variation of the resin pressure for the following cases: (1) C^o_{rr} = 14.75 kPa and n = 100 layers. (2) C^o_{rr} = 1.475 MPa and n = 50 layers. (3) C^o_{rr} = 1.475 MPa and n = 100 layers. (4) C^o_{rr} = 0.1475 GPa and n = 50 layers. (5) C^o_{rr} = 0.1475 GPa and n = 100 layers.

Table 3

Initial radial stiffness $C''_{rr}(\phi^0_s)$	Final radial stiffness $C''_{rr}(\phi_{sa})$	Δt s	Error
1.475 kPa	1.475 MPa	0.2	1.789 %
1.475 kPa	14.75 MPa	0.2	1.80 %
1.475 kPa	147.5 MPa	0.2	2.46 %
1.475 kPa	1.475 GPa	0.1	2.23 %

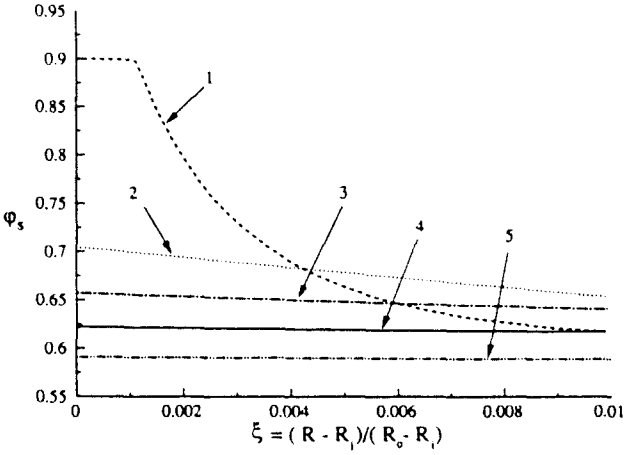

Fig. 9. Profile of fiber volume within the inner boundary layer for the following cases: (1) C''_{rr} = 1.478 kPa = constant. (2) 1.478 kPa $\leqslant C''_{rr} \leqslant$ 1.476 MPa. (3) 1.478 kPa $\leqslant C''_{rr} \leqslant$ 14.76 MPa. (4) 1.478 kPa $\leqslant C''_{rr} \leqslant$ 147.6 MPa. (5) 1.478 kPa $\leqslant C''_{rr} \leqslant$ 1.476 GPa. The number of layers n is held constant at 100.

thickness of the composite leads to increases in the level of the compressive radial stress and the resin pressure. Although the pressure distribution only shows the existence of the outer boundary layer, the actual numerical results do indicate both boundary layers. The results also indicate that for a given number of layers, increasing the radial stiffness leads to a drop in the resin pressure and an increase in the level of the compressive radial stress. When the radial resistance is sufficiently small that significant fiber compaction can take place, increasing the thickness of the cylinder leads to the expansion of the passive zone of consolidation. This can be seen from Fig. 8 where increasing the number of layers leads to the enlargement of the region in which pressure is constant†.

Figures 9–14 present the results of the numerical simulation in which the radial stiffness was allowed to vary with the fiber volume fraction. The details pertaining to the limits on the radial stiffness, the time increment and the maximum error of each calculation is shown in Table 3.

Figure 9 indicates that inclusion in the analysis of the variation of the radial stiffness with the fiber volume fraction leads to an increase in the length of the inner boundary layer. Furthermore, as Fig. 14 indicates, considering such an effect causes a non-monotonic dependence of the resin pressure on the attainable radial stiffness. This is such that increasing the maximum radial stiffness from 1.476 MPa to 147.6 MPa will actually increase the pressure inside the passive zone of the consolidation. Aside from these differences, inclusion of the variation of the instantaneous elasticity of the fiber network with fiber compaction does not alter any of the other characteristics of the solution with constant radial stiffness. For example, similar to the case of constant radial resistance, the thickness of the active region of consolidation was found to be seven to eight times the thickness of each fiber bundle. Another important common characteristic between the two classes of solutions is

†Note that based on Darcy's law (14) when the pressure is constant, the filtration flux drops to zero and hence the consolidation stops.

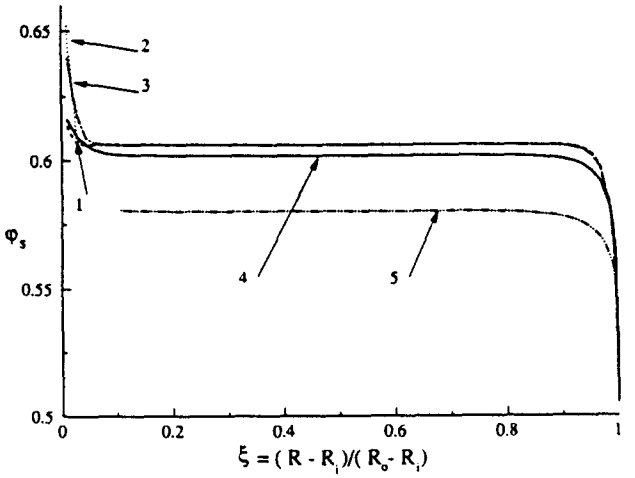

Fig. 10. Radial distribution of fiber volume fraction for the following cases: (1) C_{rr}^{o} = 1.478 kPa = constant. (2) 1.478 kPa $\leqslant C_{rr} \leqslant$ 1.476 MPa. (3) 1.478 kPa $\leqslant C_{rr} \leqslant$ 14.76 MPa. (4) 1.478 kPa $\leqslant C_{rr} \leqslant$ 147.6 MPa. (5) 1.478 kPa $\leqslant C_{rr} \leqslant$ 1.476 GPa. The number of layers is held constant at 100.

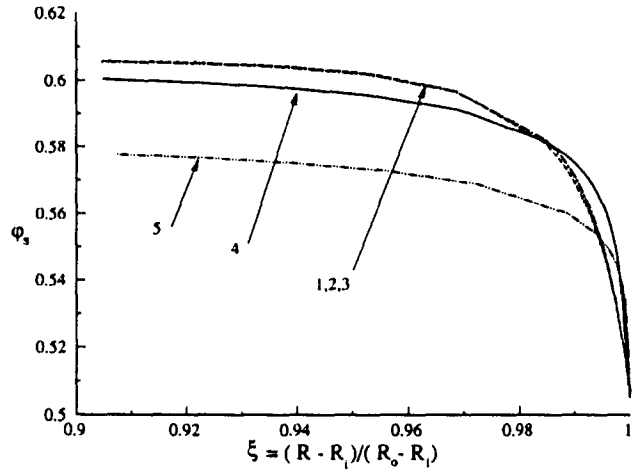

Fig. 11. Profile of fiber volume fraction within the outer boundary layer for the following cases: (1) C_{rr}^{o} = 1.478 kPa = constant. (2) 1.478 kPa $\leqslant C_{rr} \leqslant$ 1.476 MPa. (3) 1.478 kPa $\leqslant C_{rr} \leqslant$ 14.76 MPa. (4) 1.478 kPa $\leqslant C_{rr} \leqslant$ 147.6 MPa. (5) 1.478 kPa $\leqslant C_{rr} \leqslant$ 1.476 GPa. The number of layers n is held constant at 100.

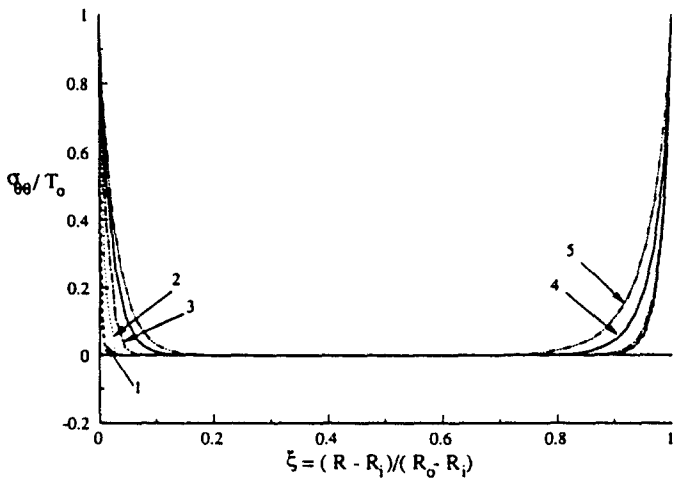

Fig. 12. Radial variation of the hoop stress for the following cases: (1) C_{rr}^{o} = 1.478 kPa = constant. (2) 1.478 kPa $\leqslant C_{rr} \leqslant$ 1.476 MPa. (3) 1.478 kPa $\leqslant C_{rr} \leqslant$ 14.76 MPa. (4) 1.478 kPa $\leqslant C_{rr} \leqslant$ 147.6 MPa. (5) 1.478 kPa $\leqslant C_{rr} \leqslant$ 1.476 GPa. The number of layers is held constant at 100.

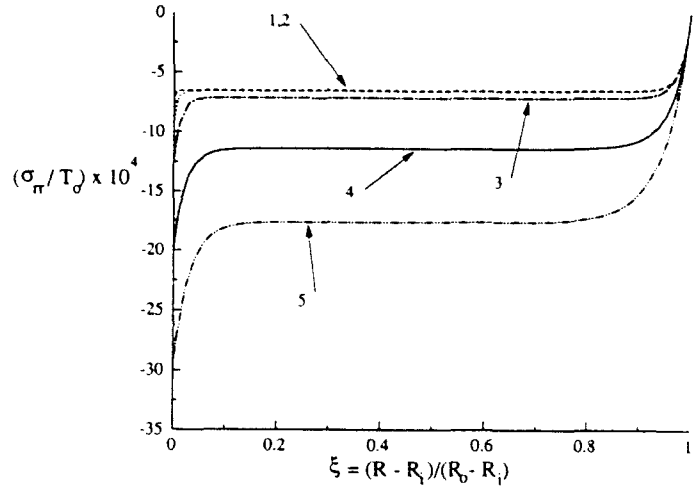

Fig. 13. Radial variation of σ_{rr} for the following cases: (1) C''_{rr} = 1.478 kPa = constant. (2) 1.478 kPa $\leqslant C_{rr} \leqslant$ 1.476 MPa. (3) 1.478 kPa $\leqslant C_{rr} \leqslant$ 14.76 MPa. (4) 1.478 kPa $\leqslant C_{rr} \leqslant$ 147.6 MPa. (5) 1.478 kPa $\leqslant C_{rr} \leqslant$ 1.476 GPa. The number of layers is held constant at 100.

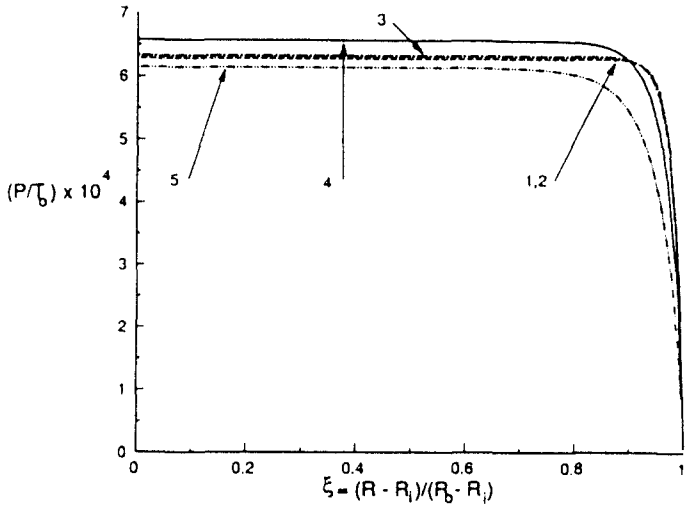

Fig. 14. Radial variation of the resin pressure for the following cases: (1) C''_{rr} = 1.478 kPa = constant. (2) 1.478 kPa $\leqslant C_{rr} \leqslant$ 1.476 MPa. (3) 1.478 kPa $\leqslant C_{rr} \leqslant$ 14.76 MPa. (4) 1.478 kPa $\leqslant C_{rr} \leqslant$ 147.6 MPa. (5) 1.478 kPa $\leqslant C_{rr} \leqslant$ 1.476 GPa. The number of layers is held constant at 100.

the existence of a radial pressure gradient following the completion of the forced winding stage. This implies that the consolidation process will continue even after the last layer has been wound onto the cylinder.

The effect of the variation of t_f/t_w on the various characteristics of the winding process is shown in Figs 15–18. Figure 15 shows that as the ratio of the filtration (consolidation) time to the winding time increases, fiber compaction decreases. This can be explained by observing that large ratios of t_f to t_w imply that as the outer radius of the cylinder increases, the resin does not have enough time to pass through the fiber network leading to small volume fractions within the cylinder. For the case under consideration, due to the fact the mandrel is assumed to be rigid, some consolidation takes place close to the mandrel–composite interface. One consequence of the delay in consolidation with increase in winding speed or decrease in permeability is the decrease in the tension drop in the radial direction, see Fig. 16. Of course one must bear in mind that due to the consolidation close to the mandrel–composite interface there is some tension drop in that region. Another consequence

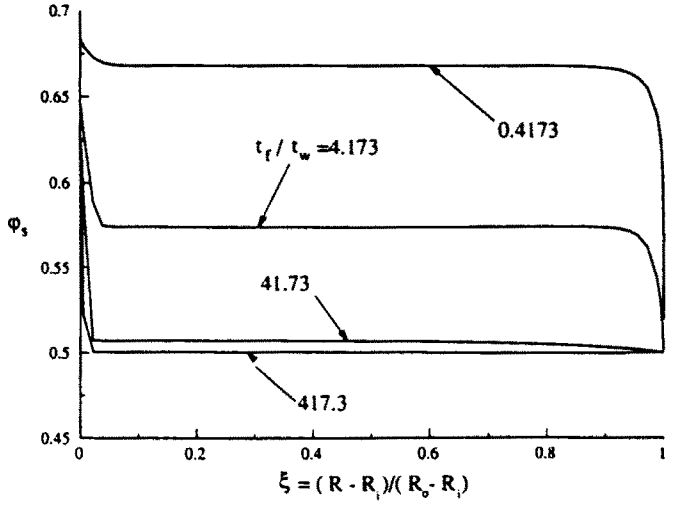

Fig. 15. Radial variation of the fiber volume fraction for different ratios of t_f/t_w. 1.478 kPa $\leqslant C_{rr} \leqslant$ 14.76 MPa and $n = 100$ layers.

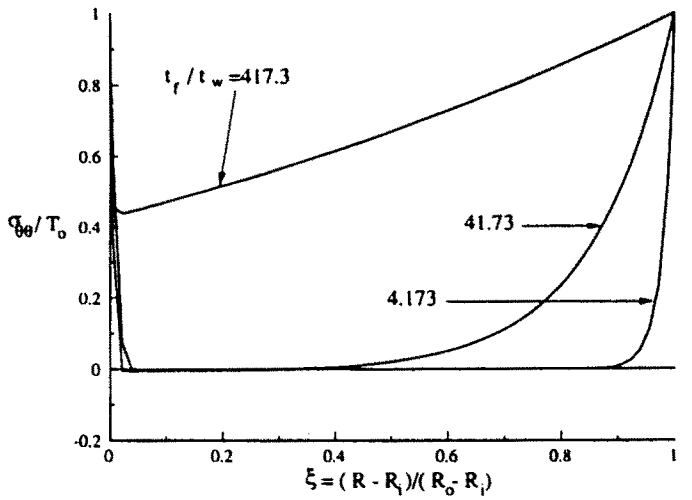

Fig. 16. Radial variation of the hoop stress for different ratios of t_f/t_w. 1.478 kPa $\leqslant C_{rr} \leqslant$ 14.76 MPa and $n = 100$ layers.

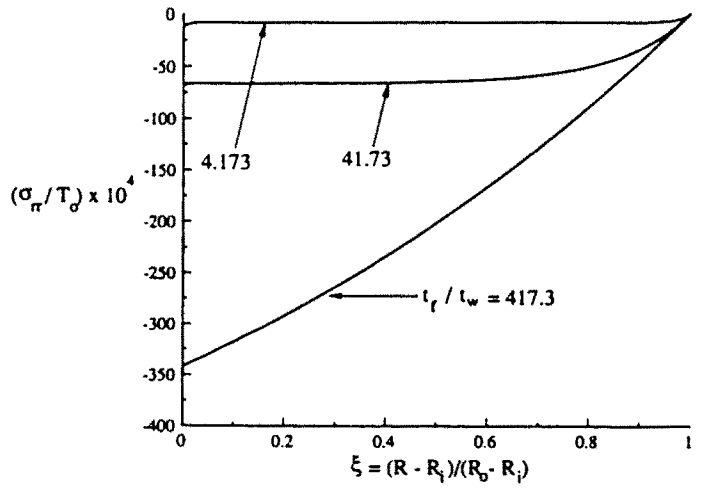

Fig. 17. Radial variation of σ_{rr} for different ratios of t_f/t_w. 1.478 kPa $\leqslant C_{rr} \leqslant$ 14.76 MPa and $n = 100$ layers.

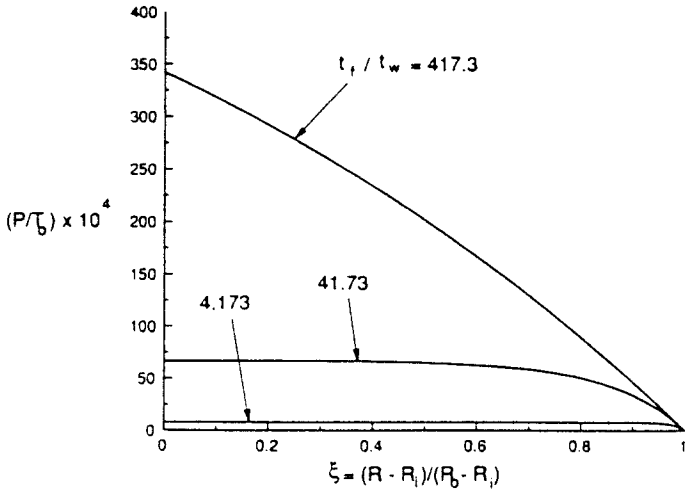

Fig. 18. Radial variation of the resin pressure for different ratios of t_f/t_w. 1.478 kPa $\leqslant C_v \leqslant$ 14.76 MPa and $n = 100$ layers.

of the delay in consolidation is the increase in the resin pressure and hence the radial stress as seen in Figs 17 and 18. Figure 18 indicates that for small ratios of t_f to t_w the active zone of consolidation is restricted to a small region close to the outer layer. As this ratio increases the length of the active zone increases and correspondingly the extent of the passive zone decreases. This is such that for substantially large values of t_f/t_w the passive zone of consolidation altogether disappears, which is a highly undesirable feature since by the time the winding stage of the manufacturing process is finished, one hopes that a major portion of consolidation is completed. Alternatively the results presented in Fig. 18 indicate that in order to increase the length of the passive zone of consolidation, one can either decrease the speed of winding or increase the permeability.

The dependence of the length of active zone of consolidation on the ratio of t_f/t_w indicates that in principle any forced winding stage belongs to one of the following three categories. First: Slow winding, where the consolidation takes place only in the last layer [Lee and Springer model; Lee and Springer (1990)]. For a given choice of fiber system, there are two circumstances under which one can have this type of winding, either the permeability is very large or the speed of winding is very small. Second: Fast winding, where either the permeability is very small (dry winding) or the speed of winding is very fast such that resin does not have enough time to filter through the fiber network. Third: Intermediate winding, where the length of the active zone of consolidation is several thicknesses of each fiber bundle wide.

6. CONCLUSION

By utilizing the rate form of the continuum mixture theory, fiber motion during wet winding of circumferentially reinforced composite cylinders is studied. The proposed formulation contains two important characteristics of this manufacturing process, namely the variation of instantaneous permeability and elasticity of the mixture with fiber compaction. In contrast to the existing models, the present formulation does not make any *a priori* assumption concerning the extent of the consolidating region. However, the model in its present form lacks the generality for analysing fiber motion and associated change in stress components in filament winding processes where the angle of winding changes.

For the case of winding onto a rigid mandrel, the numerical results, which are obtained based on a finite difference approximation, indicate that when variation of the permeability with the fiber volume fraction is taken into account there will be two distinct zones of consolidation. One in which consolidation has ceased to take place and the other inside which the fiber bundles are continuing to compact under the influence of the applied tension. Numerical results further indicate that the existence of these two regions does not depend on whether or not the increase in the radial stiffness of fiber network is taken into account.

The results further indicate that for realistic choice of the control parameters the length of the outer boundary layer within which there is active consolidation is larger than the thickness of each fiber bundle.

Based on the present results, an undesirable feature of this manufacturing process is the loss of tension in the passive zone of consolidation away from the mandrel. However, the results indicate that this drop in tension (hoop stress) decreases as the radial stiffness increases. Thus, if one is able to increase the radial stiffness through the frontal curing of the layer close to the mandrel, one will be able to reduce the drop in tension.

The results for the cases when the radial stiffness was allowed to increase from a relatively small value to a large value show that one can achieve substantial resin pressure by the end of the winding process. This is a desirable outcome since it prevents void formation during the curing process.

Further improvements on the present analysis can be achieved by developing more effective algorithms for taking into account singularity of the velocity equilibrium equation. This enables one to analyse the winding problem for arbitrary evolution of the elasticity of the network.

Acknowledgement—The authors are indebted to Professors C. L. Tucker, S. White and Dennis Parsons for valuable discussions and suggestions. The authors would also like to acknowledge helpful suggestions made by the two reviewers The work was sponsored by the National Center for Composite Materials Research at University of Illinois at Urbana-Champaign through the ONR prime contract N00014-86-K-0799.

REFERENCES

Biot, M. A. (1941). General theory of three dimensional consolidation. *J. Appl. Phys.* **12**, 155–165.

Bolotin, V. V., Vorontsov, A. N. and Murzakhanov, R. Kh. (1980). Analysis of the technological stresses in wound components made out of composites during the whole duration of the fabrication process. *Mekh. Polim.* **3**, 361–368.

Bowen, R. M. (1976). Theory of mixtures. In *Continuum Physics Part III* (Edited by Cemal Eringen), pp. 1–127. Academic Press, New York.

Calius, E. P. and Springer, G. S. (1985). Modeling the filament winding process. *Proceedings of the Fifth International Conference on Composite Materials* (Edited by W. C. Harrigan, Jr., J. Strife and A. K. Dhingra, The Metallurgical Society), pp. 1071–1088.

Calius, E. P. and Springer, G. S. (1990). Modeling of filament-wound thin cylinders. *Int. J. Solids Structures* **26**, 271–297.

Dahlquist, G. and Bjorck, A. (1974). *Numerical Methods*. Prentice-Hall, Englewood Cliffs, NJ.

Gebart, B. R. (1990). Permeability of unidirectional reinforcement for RTM. Swedish Institute for Composites, Report No. 90-006.

Gutowski, T. G., Cai, Z., Bauer, S., Boucher, D., Kingery, J. and Winman, S. (1987a). Consolidation experiments for laminate composites. *J. Comp. Mater.* **21**, 650–669.

Gutowski, T. G., Morigaki, T. and Cai, Z. (1987b). The consolidation of laminate composites. *J. Comp. Mater.* **21**, 173–188.

Kenyon, D. E. (1976). Thermostatics of solid-fluid mixtures. *Arch. Rat. Mech. Anal.* **62**, 117–129.

Lee, S. Y. and Springer, G. S. (1990). Filament winding cylinders: I. Process model. *J. Comp. Mater.* **24**, 1270–1298.

Lin, J. Y. and Westmann, R. A. (1989). Viscoelastic winding mechanics. *J. Appl. Mech.* **56**, 821–827.

Shilbey, A. M. (1982). Filament winding. In *Handbook of Composites* (Edited by G. Lubin), pp. 449–478. Nostrand-Rheinhold, New York.

Willett, M. S. and Poesch, W. L. (1988). Determining the stress distribution in wound reels of magnetic tape using a nonlinear finite-difference approach. *J. Appl. Mech.* **55**, 365–371.

APPENDIX

The elements of the tridiagonal matrix **A**, and the column vectors **B** and **R** are given as follows:

$$A_{m,m-1} = G_m^{n+1}[-\lambda c_m F_m^{n+1/2} + \lambda f_m \zeta_m + \chi_m c_m + \lambda f_m \eta_m],$$

$$A_{m,m+1} = G_m^{n+1}[-\lambda a_m F_m^{n+1/2} + \lambda d_m \zeta_m + \chi_m a_m + \lambda d_m \eta_m],$$

$$A_{m,m} = \frac{1}{\Delta y} + G_m^{n+1}\left[-\lambda b_m F_m^{n+1/2} + \frac{\phi_m^{n+1/2}}{x_m^2} + (\zeta_m + \eta_m)\left(\lambda e_m + \frac{\beta}{x_m}\right) + \chi_m\left(b_m - \frac{1}{x_m^2}\right)\right],$$

$$B_m = \frac{1}{\Delta y}\frac{G_m^{n+1}}{G_m^n}\left[W_m^n - \frac{g^n}{x_m}\right] + \frac{1}{\Delta y}\left[d_m \sigma_{rr(m+1)}^n + \left(e_m + \frac{1}{x_m}\right)\sigma_{rr(m)}^n + f_m \sigma_{rr(m-1)}^n - \frac{1}{x_m}\sigma_{\theta\theta(m)}^n\right],$$

$$R_m = \frac{1}{\Delta y x_m}. \tag{A1}$$

where

$$\zeta_m = F_m^{n+1/2}\frac{\phi_m^{n+1/2}}{\phi_m^n}(d_m F_{m+1}^n + e_m F_m^n + f_m F_{m-1}^n),$$

$$\chi_m = \frac{\Delta y}{4}F_m^{n+1}\phi_m^{n+1}\left[\lambda d_m W_{m+1}^{n+1} + \left(\lambda e_m + \frac{\beta}{x_m}\right)W_m^{n+1} + \lambda f_m W_{m-1}^{n+1}\right],$$

$$\eta_m = \frac{\Delta y}{4}F_m^{n+1}\phi_m^{n+1}\left[a_m W_{m+1}^{n+1} + \left(b_m - \frac{1}{x_m^2}\right)W_m^{n+1} + c_m W_{m-1}^{n+1}\right].$$

The above expressions are valid for all the nodal positions except the boundary nodes where one has to take account of the boundary conditions. Utilizing (32), the equivalent expressions for the nodes $m = 2$ and $m = n$ are

$$\begin{aligned} R_1 &= \left(A_{2,1} + \frac{1}{\Delta y x_2}\right), \\ R_n &= R_n - A_{n,n+1}\bar{\psi}_1, \\ A_{n,n-1} &= A_{n,n-1} - A_{n,n+1}\bar{\psi}_2, \\ A_{n,n} &= A_{n,n} - A_{n,n+1}\bar{\psi}_3, \\ B_n &= B_n + A_{n,n+1}\bar{\psi}\frac{T_0}{x_{n+1}}\frac{\mathrm{d}x_0}{\mathrm{d}y}, \end{aligned} \tag{A2}$$

where

$$\begin{aligned} \bar{\psi} &= 1\Big/\left[\frac{\mathrm{d}x_0}{\mathrm{d}y}\frac{1}{G_{n+1}^{n+1}} + \lambda d F_{n+1}^{n+1}\right], \\ \bar{\psi}_1 &= \bar{\psi}\frac{\mathrm{d}x_0}{\mathrm{d}y}\frac{1}{G_{n+1}^{n+1}x_{n+1}}, \\ \bar{\psi}_2 &= \bar{\psi}F_{n+1}^{n+1}\left(\lambda e + \frac{\beta}{x_{n+1}}\right), \\ \bar{\psi}_3 &= \bar{\psi}F_{n+1}^{n+1}\lambda f. \end{aligned}$$